Robust Rayleigh Regression Method for SAR Image Processing in Presence of Outliers

Bruna G. Palm, Fábio M. Bayer, *Member, IEEE*, Renato Machado, *Senior Member, IEEE*, Mats I. Pettersson, *Senior Member, IEEE*, Viet T. Vu, *Senior Member, IEEE*, and Renato J. Cintra, *Senior Member, IEEE*

***Abstract*— The presence of outliers (anomalous values) in synthetic aperture radar (SAR) data and the misspecification in statistical image models may result in inaccurate inferences. To avoid such issues, the Rayleigh regression model based on a robust estimation process is proposed as a more realistic approach to model this type of data. This article aims at obtaining Rayleigh regression model parameter estimators robust to the presence of outliers. The proposed approach considered the weighted maximum likelihood method and was submitted to numerical experiments using simulated and measured SAR images. Monte Carlo simulations were employed for the numerical assessment of the proposed robust estimator performance in finite signal lengths, their sensitivity to outliers, and the breakdown point. For instance, the nonrobust estimators show a relative bias value 65-fold larger than the results provided by the robust approach in corrupted signals. In terms of sensitivity analysis and break down point, the robust scheme resulted in a reduction of about 96% and 10%, respectively, in the mean absolute value of both measures, in compassion to the nonrobust estimators. Moreover, two SAR datasets were used to compare the ground type and anomaly detection results of the proposed robust scheme with competing methods in the literature.**

***Index Terms*— Outliers, Rayleigh regression model, robust estimation, synthetic aperture radar (SAR) images.**

Manuscript received March 9, 2021; revised July 12, 2021; accepted August 6, 2021. This work was supported in part by the Conselho Nacional de Desenvolvimento Científico e Tecnológico (CNPq), in part by the Coordenação de Aperfeiçoamento de Pessoal de Nível Superior (CAPES), in part by the Project Pró-Defesa IV, Brazil, in part by the Swedish-Brazilian Research and Innovation Centre (CISB), and in part by Saab AB. *(Corresponding author: Bruna G. Palm.)*

Bruna G. Palm is with the Department of Telecommunications, Aeronautics Institute of Technology (ITA), São José dos Campos 12228-900, Brazil, and also with the Department of Mathematics and Natural Sciences, Blekinge Institute of Technology, 371 79 Karlskrona, Sweden (e-mail: brunagpalm@gmail.com).

Fábio M. Bayer is with the Departamento de Estatística, Universidade Federal de Santa Maria, Santa Maria 97105-900, Brazil, and also with the Santa Maria Space Science Laboratory (LACESM), Universidade Federal de Santa Maria, Santa Maria 97105-900, Brazil (e-mail: bayer@ufsm.br).

Renato Machado is with the Department of Telecommunications, Aeronautics Institute of Technology (ITA), São José dos Campos 12228-900, Brazil (e-mail: rmachado@ita.br).

Mats I. Pettersson and Viet T. Vu are with the Department of Mathematics and Natural Sciences, Blekinge Institute of Technology, 371 79 Karlskrona, Sweden (e-mail: mats.pettersson@bth.se; viet.thuy.vu@bth.se).

Renato J. Cintra is with the Signal Processing Group, Departamento de Estatística, Universidade Federal de Pernambuco, Recife 50670-901, Brazil, and also with the Department of Electrical and Computer Engineering, Florida International University, Miami, FL 33199 USA (e-mail: rjdsc@de.ufpe.br).

Digital Object Identifier 10.1109/TGRS.2021.3105694

I. Introduction

SYNTHETIC aperture radar (SAR) data play an important role in remote sensing applications [1] due to its capability of providing: 1) wide terrain coverage in a short observation of time and 2) suitable visual information acquisition, independent of weather and illumination conditions [2]. However, SAR images are frequently contaminated by a percentage of outliers (anomalous values)—image pixels that differ significantly from their neighborhood [3]—which can be related to human-made objects or highly reflective areas [4]. Because such observations do not follow the general behavior of the neighborhood or the observed scene [2], the use of suitable approaches to deal with outliers should be considered to avoid unreliable results in remote sensing applications [4]. For example, in [5], the median was employed to obtain a ground scene predicted (GSP) image based on an image stack of the CARABAS II dataset [6]. The resulted image was applied as a reference image in a change detection algorithm. The median is a robust method and was considered in the CARABAS II SAR image dataset to remove outliers (military vehicles), resulting in high probability detection values, associated with low false alarm rates, highlighting the importance of robust methods to deal with outliers.

Typical tasks in SAR data analysis and processing include: 1) image modeling [7], [8]; 2) identification and classification of distinct ground type [9], [10]; and 3) change detection [11], [12]. The use of statistical models—commonly employed to describe image pixels by a small number of parameters [13]—can generate accurate results for the above SAR-related challenges, as presented in [14] and [15]. The statistical inference methods widely considered for signal and image modeling usually suppose: 1) Gaussian or symmetric data [13], [16] and 2) least-squares or maximum likelihood approaches [13].

However, magnitude SAR image pixels generally present non-Gaussian properties, such as asymmetrical distributions and strictly positive values [1]. These characteristics motivated the proposition of a regression model based on the Rayleigh distribution for SAR image modeling [17]. The Rayleigh regression model is suitable for non-Gaussian situations, where the observed output signal is asymmetric and measured continuously on the real positives values, such as SAR amplitude image pixels. The Rayleigh regression model assumes that the Rayleigh distributed signal mean follows a

regression structure involving covariates, unknown parameters, and a link function. In [17], an inference approach for the model parameters, diagnostic tools, asymptotic proprieties of the parameter estimators, and a ground type detector were discussed. In addition, as in other classes of non-Gaussian regression models, such as the generalized linear model [18], the Rayleigh regression model was derived considering the maximum likelihood approach to estimate its parameters. However, robust tools were not discussed.

The maximum likelihood inference method is asymptotically efficient but lacks robustness against model misspecification and outliers [16], [19]. On the other hand, robust approaches are not significantly affected by outliers or small model departures [16]. Consequently, aiming at avoiding corrupted results related to the presence of outliers in the signal of interest, robust approaches for the ordinary linear regression models and generalized linear models have been discussed (see [19] and [20]). In addition, as discussed in [21], robustness is an important feature to obtain meaningful physical estimated parameters in remotely sensed data since robust statistical processing involves making inferences in distorted or corrupted signals [16], [22], such as SAR data.

In [5], the median was applied in an image stack to obtain a GSP image, while, in [17], the Rayleigh regression model was introduced; both schemes were considered in remote sensing applications. In particular, the GSP image was employed in a change detection algorithm, and the Rayleigh regression model was considered in a ground type detection tool. However, to the best of our knowledge, a robust approach for the Rayleigh regression model parameter estimation is absent in the literature, and this article aims at proposing the first treatment. In this article, our goal is twofold. First, we derive a robust statistical tool for the Rayleigh regression model for corrupted signals. Specifically, to obtain the parameter estimators robust to the presence of outliers, we employed the weighted maximum likelihood method [23]. We introduce parameter estimation and large data record inference. Monte Carlo simulations are used to evaluate the finite signal length performance of the Rayleigh regression model robust parameter estimators, its sensitivity to outliers, and the breakdown point. Second, this article attempts to establish a framework for detection tools in SAR images corrupted with outliers according to the following methodology.

1) We use the proposed robust approach to detect ground types in the magnitude single-look SAR images obtained from
   1) CARABAS II, a Swedish ultrawideband (UWB) very-high frequency (VHF) SAR system.
   2) OrbiSAR, a Brazilian SAR system operating at X- and P-bands.
2) We employ the introduced robust scheme to detect targets in a CARABAS II SAR image since this dataset is widely explored in the literature for detection of military vehicles concealed by forest (see [5], [6], [24], [25], and [26]). Such targets can be interpreted as anomalies since they introduce more representative behavior changes in the CARABAS II ground scene.

The article is organized as follows. Section II reviews the Rayleigh regression model and introduces robust parameter estimation and large data record properties. Section III shows a Monte Carlo simulation study for numerical evaluation of the introduced approach, using breakdown point and sensitivity analysis. Section IV displays two experiments with two measured SAR datasets. Finally, the conclusion of this work can be found in Section V.

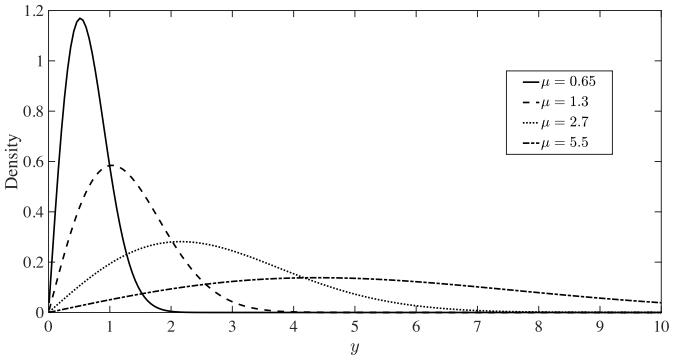

Fig. 1. Rayleigh probability density functions for $\mu \in \{0.65, 1.3, 2.7, 5.5\}$.

II. Proposed Robust Rayleigh Regression Method

This section introduces a robust estimation approach for the Rayleigh regression model parameters based on the weighted maximum likelihood method. Moreover, large data record inferences are discussed.

A. Rayleigh Regression Model

The Rayleigh regression model introduced in [17] can be defined as follows. Let $Y[n]$, $n = 1, 2, \ldots, N$, be a Rayleigh distributed random variable, and let $y[n]$ be the realization of the signal $Y[n]$ with mean $\mu[n]$. Considering the mean-based parametrization of $Y[n]$, we have that the probability density function of $Y[n]$ is written as

$$f_Y(y[n];\, \mu[n]) = \frac{\pi\, y}{2\mu[n]^2} \exp\left(-\frac{\pi\, y[n]^2}{4\mu[n]^2}\right) \tag{1}$$

where $E(Y[n]) = \mu[n] > 0$. Also, we have that $\mathrm{Var}(Y[n]) = \mu[n]^2((4/\pi) - 1)$. Fig. 1 shows a few different Rayleigh densities along with the corresponding mean parameter (μ) values. It is noteworthy that the Rayleigh distribution is flexible, displaying different shapes depending on the mean parameter value. The cumulative distribution function and the quantile function are provided, respectively, by

$$F_Y(y[n];\, \mu[n]) = 1 - \exp\left(-\frac{\pi\, y[n]^2}{4\mu[n]^2}\right) \tag{2}$$

$$Q_Y(u[n];\, \mu[n]) = 2\mu[n]\sqrt{\frac{-\log(1-u[n])}{\pi}}. \tag{3}$$

The quantile function is useful for generating nonuniform pseudorandom occurrences according to the inversion method—probability integral transform (PIT)—which involves computing the quantile function and then inverting it [27, Ch. 2]. The cumulative distribution function is employed to define the quantile residuals [28], which is derived based on $F_Y(y[n];\, \mu[n])$ and standard normal quantile function. Both

methods are considered in the simulation and SAR image studies presented in this article.

The Rayleigh regression model is defined, assuming that the mean $\mu[n]$ of the observed output signal $Y[n]$ can be written as

$$\eta[n] = g(\mu[n]) = \sum_{i=1}^{k} \beta_i x_i[n], \quad n = 1, 2, \ldots, N \tag{4}$$

where $k < N$ is the number of covariates considered in the model, $\boldsymbol{\beta} = (\beta_1, \beta_2, \ldots, \beta_k)^\top$ is the vector of unknown parameters, $\mathbf{x}[n] = (x_1[n], x_2[n], \ldots, x_k[n])^\top$ is the vector of deterministic independent input variables, $g : \mathbb{R}^+ \to \mathbb{R}$ is a strictly monotonic and twice differentiable link function, and $\eta[n]$ is the linear predictor. Parameter estimation based on the maximum likelihood method, diagnostic measures, and further mathematical properties, including large data record results, are fully discussed in [17].

B. Robust Estimation

Robust parameter estimation of the Rayleigh regression model can be performed by the weighted maximum likelihood approach [23]. Given a known weighted vector $\mathbf{w} = (w[1], w[2], \ldots, w[N])^\top$, the weighted maximum likelihood estimates are given by

$$\widehat{\boldsymbol{\beta}} = \arg\max_{\boldsymbol{\beta}} \ell_w(\boldsymbol{\beta}) \tag{5}$$

where $\ell_w(\boldsymbol{\beta})$ is the weighted log-likelihood function of the parameters for the observed signal, defined as

$$\ell_w(\boldsymbol{\beta}) = \sum_{n=1}^{N} w[n]\ell[n](\mu[n]). \tag{6}$$

The quantity $\ell[n](\mu[n])$ is the logarithm of $f(y[n], \mu[n])$, which is written as

$$\ell[n](\mu[n]) = \log\left(\frac{\pi}{2}\right) + \log(y[n]) - \log(\mu[n]^2) - \frac{\pi y[n]^2}{4\mu[n]^2} \tag{7}$$

where $\mu[n] = g^{-1}(\sum_{i=1}^{k} x_i[n]\beta_i)$. The weighted score vector, obtained by differentiating the weighted log-likelihood function with respect to each unknown parameters β_i, $i = 1, 2, \ldots, k$, is given by

$$U_w(\boldsymbol{\beta}) = \left(\frac{\partial \ell_w(\boldsymbol{\beta})}{\partial \beta_1}, \frac{\partial \ell_w(\boldsymbol{\beta})}{\partial \beta_2}, \ldots, \frac{\partial \ell_w(\boldsymbol{\beta})}{\partial \beta_k}\right)^\top. \tag{8}$$

Considering the chain rule, we have that

$$\frac{\partial \ell_w(\boldsymbol{\beta})}{\partial \boldsymbol{\beta}} = \sum_{n=1}^{N} w[n] \frac{d\ell[n](\mu[n])}{d\mu[n]} \frac{d\mu[n]}{d\eta[n]} \frac{\partial \eta[n]}{\partial \boldsymbol{\beta}}. \tag{9}$$

As reported in [17], note that

$$\frac{d\ell[n](\mu[n])}{d\mu[n]} = \frac{\pi y[n]^2}{2\mu[n]^3} - \frac{2}{\mu[n]} \tag{10}$$

$$\frac{d\mu[n]}{d\eta[n]} = \frac{1}{g'(\mu[n])} \tag{11}$$

$$\frac{\partial \eta[n]}{\partial \beta_i} = x_i[n] \tag{12}$$

where $g'(\cdot)$ is the first derivative of the adopted link function $g(\cdot)$. In the matrix form, the weighted score vector can be written as

$$U_w(\boldsymbol{\beta}) = \mathbf{X}^\top \cdot \mathbf{W} \cdot \mathbf{T} \cdot \mathbf{v} \tag{13}$$

where $\mathbf{X}$ is an $N \times k$ matrix whose nth row is $\mathbf{x}[n]^\top$, and

$$\mathbf{W} = \text{diag}\{w[1], w[2], \ldots, w[N]\},$$

$$\mathbf{T} = \text{diag}\left\{\frac{1}{g'(\mu[1])}, \frac{1}{g'(\mu[2])}, \ldots, \frac{1}{g'(\mu[N])}\right\},$$

$$\mathbf{v} = \left(\frac{\pi y[1]^2}{2\mu[1]^3} - \frac{2}{\mu[1]}, \frac{\pi y[2]^2}{2\mu[2]^3} - \frac{2}{\mu[2]}, \ldots, \frac{\pi y[N]^2}{2\mu[N]^3} - \frac{2}{\mu[N]}\right)^\top.$$

Thus, the weighted maximum likelihood estimator (WMLE) for each Rayleigh regression model parameter is obtained by solving the following nonlinear system:

$$U_w(\boldsymbol{\beta}) = \mathbf{0} \tag{14}$$

where $\mathbf{0}$ is the k-dimensional vector of zeros. The quasi-Newton Broyden–Fletcher–Goldfarb–Shanno (BFGS) method [29] with analytic first derivatives was considered as the nonlinear optimization algorithm to solve (14). To determine the initial points, we followed the same methodology described in [17].

1) Weighted Vector Determination: The WMLE is obtained supposing that the weights $w[n]$, $n = 1, 2, \ldots, N$, are known. However, in practice, we have to determine these values. As suggested by [23], we consider the following approach for the weighted vector determination:

$$w[n] = \begin{cases} \dfrac{F(y[n]; \mu[n])}{\delta}, & \text{if } F(y[n]; \mu[n]) < \delta \\ 1, & \text{if } \delta \le F(y[n]; \mu[n]) \\ & \le 1 - \delta \\ \dfrac{1 - F(y[n]; \mu[n])}{\delta}, & \text{if } F(y[n]; \mu[n]) > 1 - \delta \end{cases} \tag{15}$$

where $\delta \in (0, 1)$ is employed to delimit the weighed distribution interval in $(1 - 2\delta)\%$ and the unknown parameter is replaced by their nonrobust maximum likelihood estimator (MLE). Typical values for δ are 0.01 and 0.001 [23]. We note that atypical $y[n]$ values imply in large or small $F(y[n]; \mu[n])$ values, which are weighted; consequently, inference distortions related to these observations are minimized.

C. Testing Inference

Under the following mild regularity conditions: 1) the first- and second-order derivatives of the weighted log-likelihood function are well-defined and 2) the expectation of the score function is equal to zero, it is shown in [23] and [30] that the WMLEs are asymptotically equivalent to the MLEs. Thus, we can use the classical Wald statistic to make inferences about the regression parameters. Suppose that we partition the parameter vector $\boldsymbol{\beta}$ into a vector of parameters of interest ($\boldsymbol{\beta}_I$), with dimension ν, and in a nuisance parameter vector ($\boldsymbol{\beta}_M$), with dimension $k - \nu$. The interest hypothesis $\mathcal{H}_0$ and the alternative hypothesis $\mathcal{H}_1$ are given by

$$\begin{cases} \mathcal{H}_0 : \boldsymbol{\beta}_I = \boldsymbol{\beta}_{I0} \\ \mathcal{H}_1 : \boldsymbol{\beta}_I \neq \boldsymbol{\beta}_{I0} \end{cases} \tag{16}$$

where $\boldsymbol{\beta}_{I0}$ is a fixed column vector of dimension ν. The Wald statistic is given by [31]

$$T_W = \left(\widehat{\boldsymbol{\beta}}_{I1} - \boldsymbol{\beta}_{I0}\right)^{\top} \left(\left[\mathbf{I}^{-1}\left(\widehat{\boldsymbol{\beta}}_1\right)\right]_{\beta_I \beta_I}\right)^{-1} \left(\widehat{\boldsymbol{\beta}}_{I1} - \boldsymbol{\beta}_{I0}\right) \quad (17)$$

where $\widehat{\boldsymbol{\beta}}_1 = (\widehat{\boldsymbol{\beta}}_{I1}^{\top}, \widehat{\boldsymbol{\beta}}_{M1}^{\top})^{\top}$ is the WMLE under $\mathcal{H}_1$, $\mathbf{I}(\widehat{\boldsymbol{\beta}})$ is the Fisher information matrix derived in [17] evaluated at the WMLE, and $[\mathbf{I}^{-1}(\widehat{\boldsymbol{\beta}})]_{\beta_I \beta_I}$ is a partition of $\mathbf{I}(\widehat{\boldsymbol{\beta}})$ limited to the interest estimates. The Fisher information matrix is given by $\mathbf{I}(\boldsymbol{\beta}) = \mathbf{X}^{\top} \cdot \mathbf{W} \cdot \mathbf{X}$, where

$$\mathbf{W} = \operatorname{diag}\left\{ \frac{4}{\mu[1]^2}\left(\frac{d\mu[1]}{d\eta[1]}\right)^2, \frac{4}{\mu[2]^2}\left(\frac{d\mu[2]}{d\eta[2]}\right)^2, \ldots, \times \frac{4}{\mu[N]^2}\left(\frac{d\mu[N]}{d\eta[N]}\right)^2 \right\}. \quad (18)$$

In particular, for the log link function ($g(\mu[n]) = \log(\mu[n])$), the Fisher information matrix is exactly the same for the robust and nonrobust approaches, since $(d\mu[n]/d\eta[n]) = \mu[n]$.

Based on the consistency of the WMLE and the asymptotic normality of the estimators, T_W statistic follows, in large data records, a chi-square distribution with ν degrees of freedom, χ^2_{ν}. The test is performed by comparing the calculated value of T_W with a threshold value, γ, obtained from the χ^2_{ν} distribution and the desired probability of false alarm [31]. The Wald test described above can be used for several detection signal applications, such as ground type use and the presence of a signal.

III. Simulation Study

This section considers Monte Carlo simulations to evaluate the finite signal length performance of the robust point estimators of the Rayleigh regression model parameters. For such, we assess the estimation performance with and without outliers. We also measure the estimator sensitivity in the presence of anomalous observations and the breakdown point.

A. Robust Point Estimators' Performance

The numerical evaluation was made over 5000 different signal samples generated by means of (4) and considering the log link function. Following the methodology described in [17], the parameters were adopted as follows: $\beta_1 = 0.5$ and $\beta_2 = 0.15$, and the covariate was obtained from the uniform distribution $(0, 1)$ and considered constants for all Monte Carlo replications. In each replication, the inversion method was employed to simulate $y[n]$ assuming the Rayleigh distribution with mean $\mu[n] = \exp\{\beta_1 + \beta_2\ x_2[n]\}$.

The simulation study considered signals in several situations, varying the sample size $N \in \{100, 500, 750\}$ and the contamination level $\epsilon \in \{0\%, 1\%, 5\%\}$. The selected values of ϵ follow the literature, as shown in [7], [32], and [33] for robust estimation analysis in 1-D, 2-D, and 3-D models, respectively. The outliers were included, assuming a value equal to 10 in randomized positions. We employed $\delta \in \{0.001, 0.01\}$ for the weight determination; however, for brevity and similarity of results, just the ones for $\delta = 0.001$ are shown. The percentage relative bias (RB%), the mean square error (MSE), and the sum of the absolute values of RB% and MSE total were adopted as figures of merit to numerically evaluate the proposed robust estimators. Such error measures are expected to be as small as possible and were computed between $\boldsymbol{\beta}$ and $\widehat{\boldsymbol{\beta}}$.

Table I shows the Monte Carlo simulation results for the point estimators of the Rayleigh regression model parameters with and without outliers. Both WMLEs and MLEs show similar and small values of RB% and MSE for the data without outliers. In particular, the absolute total value of relative bias for $N = 100$ is equal to 1.6228 and 1.5765 for WMLE and MLE, respectively. However, the MLEs present higher values of RB% and MSE for the contaminated data when compared to the WMLE results, showing that the robust theory is effective, reducing considerably the RB% and MSE values concerning the nonrobust estimation method in corrupted signals. For instance, consider the case with 5% of contamination and $N = 500$, and the WMLE for β_1 displays values of RB% equal to 1.8567%, while the MLE shows RB% value about 106% for the same parameter. Summarizing, the WMLEs show either equal or better performance compared with the results from the MLEs, in all evaluated cases.

B. Breakdown Point and Sensibility Curve

The breakdown point was proposed in [34] and evaluate the proportion of outliers that the signal may contain such that $\widehat{\boldsymbol{\beta}}$ still provides some information about the true parameter [16], [34], [35]. Fig. 2(a) displays the total breakdown point in terms of the total relative bias of the estimators, which is defined as the sum of the absolute values of the individual relative biases. As in the robust estimators' point evaluation, the outlier value was set equal to 10. In addition, we employed 1000 Monte Carlo replications and the number of outliers ranging from 1 to 100. We note that the WMLEs show smaller total relative bias values compared with the results from the MLEs, in all evaluated cases. In general, we note that, for 1% of contamination, the MLEs present total relative bias close to or higher than 100. On the other hand, the WMLEs show the same total relative bias values for a contamination level of about 10% of the observations.

Another measure widely used to evaluate robust estimators is the sensitivity curve (SC) [16], which provides an intuitive information about the sensitivity of an estimator measuring its variability with the addition of an outlier to the signal. The SC is given by [16]

$$\mathrm{SC}(\mathbf{y}, \widehat{\boldsymbol{\beta}}) = N \cdot \left(\widehat{\boldsymbol{\beta}}(y[1], y[2], \ldots, y[N-1], y_{\text{out}}) - \widehat{\boldsymbol{\beta}}(y[1], y[2], \ldots, y[N-1])\right) \quad (19)$$

where $\widehat{\boldsymbol{\beta}}(y[1], y[2], \ldots, y[N-1])$ is the estimator without outliers and $\widehat{\boldsymbol{\beta}}(y[1], y[2], \ldots, y[N-1], y_{\text{out}})$ is the estimator contaminated with an outlier y_{out}. For a better graphical analysis, the SC results are shown as the mean absolute value of SC (MASC) of all estimators. This unified measure was proposed in [33] for multiparametric evaluations.

TABLE I

RESULTS OF THE MONTE CARLO SIMULATION OF THE POINT ESTIMATION CONSIDERING THE ROBUST (WMLE) AND NONROBUST (MLE) APPROACHES, WITH AND WITHOUT OUTLIERS, FOR $\beta_1 = 0.5$, $\beta_2 = 0.15$, AND $\delta = 0.001$

		WMLE			MLE		
ϵ	Measures	$\widehat{\beta}_1$	$\widehat{\beta}_2$	Absolute Total	$\widehat{\beta}_1$	$\widehat{\beta}_2$	Absolute Total
				$N = 100$			
0%	Mean	0.4957	0.1488	—	0.4967	0.1486	—
	RB(%)	−0.8570	−0.8259	1.6828	−0.6598	−0.9167	1.5765
	MSE	0.0100	0.0312	0.0413	0.0099	0.0309	0.0409
1%	Mean	0.4968	0.1480	—	0.6401	0.1247	—
	RB(%)	−0.6311	−1.3311	1.9622	28.0262	−16.8944	44.9206
	MSE	0.0101	0.0316	0.0417	0.0715	0.1916	0.2631
5%	Mean	0.5476	0.1597	—	1.0103	0.0705	—
	RB(%)	9.5122	6.4767	15.9889	102.0672	−53.0026	155.0698
	MSE	0.0518	0.1693	0.2211	0.3405	0.3098	0.6503
				$N = 500$			
0%	Mean	0.4974	0.1508	—	0.4989	0.1508	—
	RB(%)	−0.5234	0.5316	1.0550	−0.2291	0.5216	0.7507
	MSE	0.0021	0.0062	0.0083	0.0020	0.0061	0.0081
1%	Mean	0.4989	0.1506	—	0.6579	0.1183	—
	RB(%)	−0.2117	0.4203	0.6320	31.5790	−21.1080	52.6870
	MSE	0.0021	0.0062	0.0083	0.0362	0.0425	0.0786
5%	Mean	0.5093	0.1628	—	1.0314	0.0679	—
	RB(%)	1.8567	8.5400	10.3967	106.2793	−54.7086	160.9879
	MSE	0.0045	0.0162	0.0208	0.2954	0.0566	0.3519
				$N = 750$			
0%	Mean	0.4980	0.1507	—	0.4996	0.1506	—
	RB(%)	−0.3962	0.4568	0.8530	−0.0875	0.4140	0.5015
	MSE	0.0014	0.0041	0.0054	0.0014	0.0040	0.0054
1%	Mean	0.4997	0.1507	—	0.6673	0.1184	—
	RB(%)	−0.0593	0.4608	0.5201	33.4529	−21.0987	54.5516
	MSE	0.0014	0.0041	0.0054	0.0360	0.0300	0.0660
5%	Mean	0.5080	0.1631	—	1.0359	0.0698	—
	RB(%)	1.6012	8.7438	10.3450	107.1780	−53.4431	160.6211
	MSE	0.0027	0.0099	0.0127	0.2959	0.0396	0.3355

The MASC considering 5% of outliers with their values ranging from 1 to 20 and 1000 Monte Carlo replications is presented in Fig. 2(b), showing that the WMLE is more robust to outliers compared to the MLE for all evaluated outlier values and signal lengths. The MLE displays a MASC maximum value of about 130, while the WMLE does not show values higher than 5. In addition, the WMLEs present similar behavior regardless of the evaluated signal length and outlier value, whereas the MLEs display higher MASC values as the signal length and the outlier value increase.

In summary, the Monte Carlo simulations show that the robust-based Rayleigh regression model parameter estimators are not strongly influenced by the presence or absence of outliers in the observed signal. Furthermore, in real-world scenarios, identifying whether a signal is contaminated by outliers is not an easy task. Thus, using a robust approach to estimate the parameters of the Rayleigh regression model can avoid inaccurate inferences.

IV. SAR IMAGE STUDY

In this section, experiments with two measured SAR datasets are presented to demonstrate the applicability of the proposed approach in the SAR image analysis. We employed the introduced robust scheme to detect the ground type and anomalies in SAR image scenes. In particular, VHF wavelength-resolution SAR images are almost speckle-free since there might only be a single scatter in the resolution cell (at least for the CARABAS II dataset). On the other hand, nonwavelength-resolution SAR images are characterized by the possible presence of more than one strong scatter in the resolution cell area, which makes the speckle noise not negligible. We emphasize that the speckle and other random effects are accommodated in the Rayleigh-distributed output signal $Y[n]$. The regression structure models the mean of $Y[n]$, which is deterministically affected by parameters and known covariates (input).

A. Ground Type Detector

In this experiment, we considered the ground type detection methodology used in [17] to distinguish between three regions in two SAR images extracted from CARABAS II and OrbiSAR datasets considering the proposed robust approach.

1) CARABAS II: As reported in [6] and [24], the CARABAS II is a VHF wavelength-resolution system, which

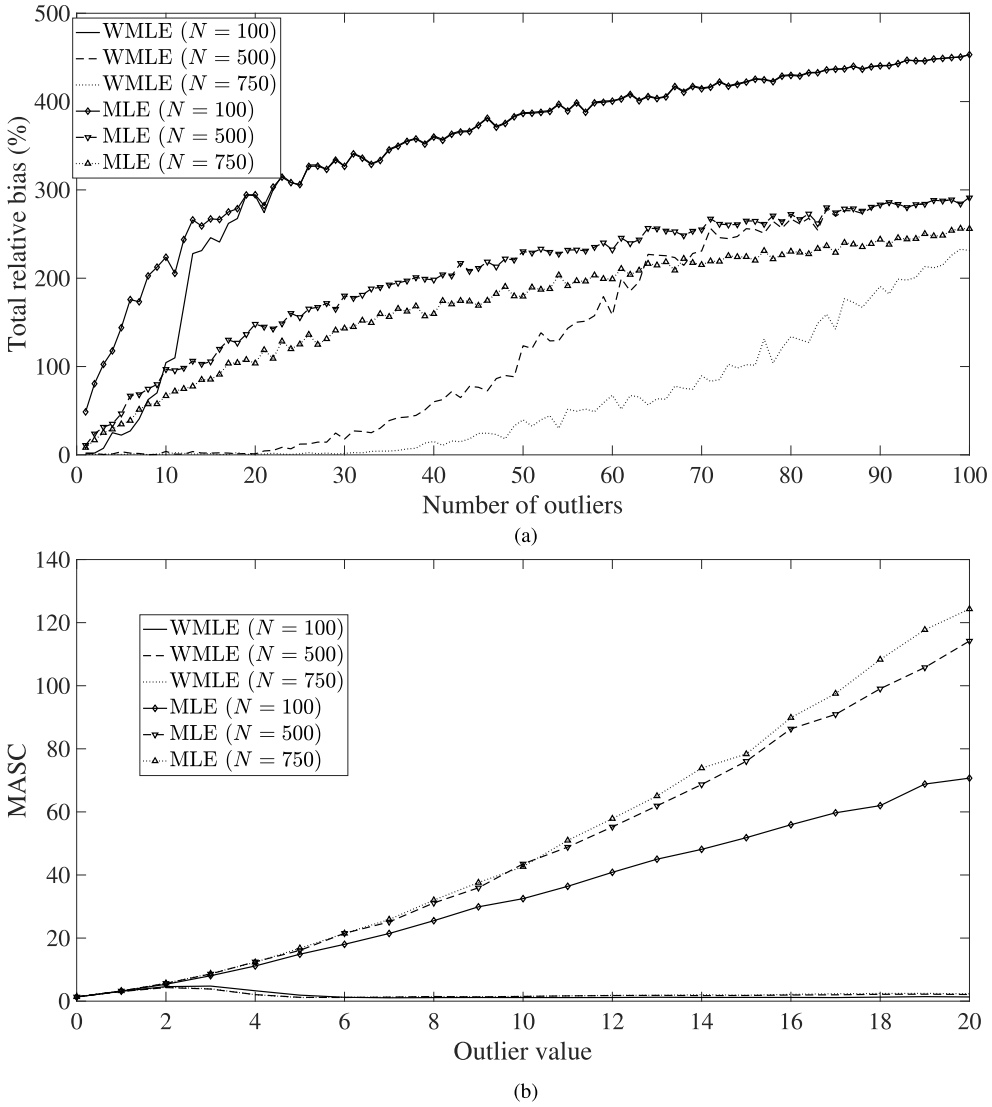

Fig. 2. Total breakdown point and sensitivity results considering 5% of outliers and 1000 Monte Carlo replications. (a) Total breakdown point. (b) Sensitivity curves (SCs).

means that the images have almost no speckle noise. The system operates with horizontal (HH) polarization, and the spatial resolution is 2.5 m in both azimuth and slant ranges. The CARABAS II images are: 1) represented as matrices of 3000 × 2000 pixels (each pixel size is 1 m × 1 m), corresponding to an area of 6 km^2, and covering a scene of size 3 km × 2 km; 2) georeferenced to the Swedish reference system RR92; and 3) available in [36].

The ground scene is dominated by a boreal forest with pine trees. Fences, power lines, and roads were also present in the scene. Military vehicles (targets) were deployed in the SAR scene and placed uniformly in a manner to facilitate their detection in the tests [6]. The image has 25 targets of three different sizes, and the spacing between the vehicles is about 50 m.

In [17], the difference in the behavior among the lake, forest, and military vehicles' regions was computed. The forest and lake regions in the CARABAS II SAR image characterize most of the image area, and they follow a homogeneous pattern. The military vehicles deployed in the SAR scene introduce more representative behavior changes compared to the forest and lake regions (homogeneous areas). In addition, pixels related to the power lines show similar amplitude values with the targets and, consequently, are strongly related to the false alarm detection in this particular dataset, as discussed in [6]. Furthermore, as both targets and power line structures present a different pattern from the rest of the image, they may be considered as anomalies observations (outliers).

Thus, we adopted the detection methodology proposed in [17] to distinguish among an area containing military vehicles, power lines, and forests—referred to as Regions A, B, and C, respectively—which are displayed in Fig. 3. For such, we modeled the response signal mean considering an intercept, $x_1[n] = 1, \ \forall n$, and two dummy variables, $x_2[n]$ and $x_3[n]$, representing each evaluated region. The fit model is given by

$$g(\mu[n]) = \beta_1 + \beta_2 x_2[n] + \beta_3 x_3[n] \tag{20}$$

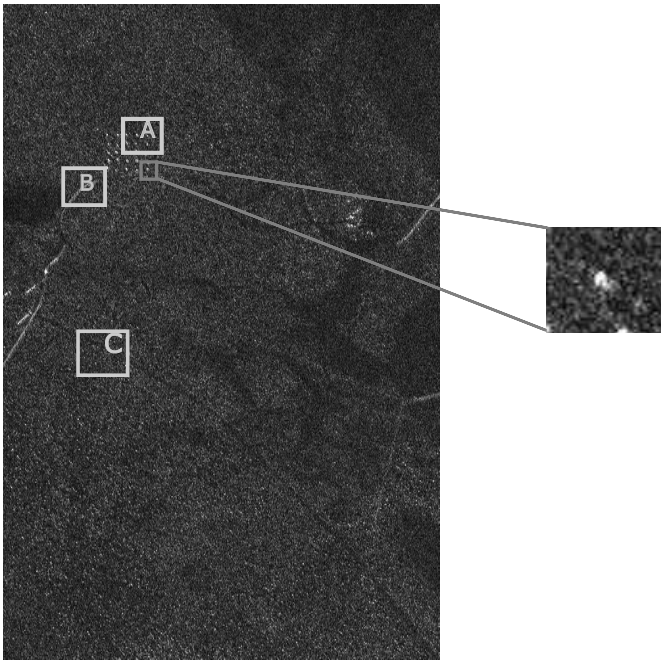

Fig. 3. CARABAS II image used in the regression models showing the tested regions. Regions A, B, and C represent areas containing military vehicles, power lines, and forest, respectively.

where: 1) $y[n]$ is the vectorized magnitude pixels of Regions A, B, and C; 2) variable $x_2[n] = 1$, for Region B, and zero for the rest; 3) variable $x_3[n] = 1$, for Region C, and zero for the others; and 4) Region A is represented for both $x_2[n]$ and $x_3[n]$ equal to zero.

To detect the ground type, the following hypotheses are tested:

$$\begin{cases} \mathcal{H}_0 : \beta_i = 0 \\ \mathcal{H}_1 : \beta_i \neq 0 \end{cases} \tag{21}$$

for $i = 2, 3, \ldots, k$. The evaluated ground types are detected when the null hypothesis (21) is rejected, i.e., $T_W > \gamma$. We also obtained the detection results based on: 1) the Gaussian and Gamma regression models considering a robust estimation process and 2) the Rayleigh regression model based on the maximum likelihood estimation scheme for comparative purposes. To implement the detectors through the Gaussian- and Gamma-based regression models considering a robust approach, the `R` function `glmrob` [37] was used. To perform the ground type detection, the probability of false alarm was fixed to 0.05, which is a convenient cutoff level to reject the null hypothesis [38], and it is widely employed in signal detection applications [39]–[42].

The fit models can be found in Table II. Note that the estimated values are not the same as those presented in [17], since we evaluated different regions in the present experiment. To perform the robust estimation in the Rayleigh regression model, we employed $\delta = 0.001$. Considering a probability of false alarm equal to 0.05, the p-values of the Wald test presented in Table II show that all variables in the proposed robust scheme are significant, i.e., the null hypothesis in (21) can be rejected, and consequently, a correct detection of all evaluated land types is indicated. On the other hand, the variable $x_2[n]$ is not significant for the other evaluated regression models, i.e., the Rayleigh regression model based on the nonrobust estimation process and the models using the Gaussian and Gamma based on a robust estimation process cannot distinguish the power line regions, showing the importance of robust methods based on suitable distributions to deal with outliers in SAR image modeling.

TABLE II
FIT REGRESSION MODELS FOR REGIONS A, B, AND C

	Estimate	Standard Error	p-value
Rayleigh regression model (robust estimators)			
$\widehat{\beta}_1$	-1.6681	0.0333	< 0.001
$\widehat{\beta}_2$	0.1168	0.0521	0.0250
$\widehat{\beta}_3$	-0.4993	0.0521	< 0.001
Rayleigh regression model (non-robust estimators)			
$\widehat{\beta}_1$	-1.4916	0.0333	< 0.001
$\widehat{\beta}_2$	-0.0555	0.0521	0.2867
$\widehat{\beta}_3$	-0.6759	0.0521	< 0.001
Gaussian regression model (robust estimators)			
$\widehat{\beta}_1$	0.1896	0.0090	< 0.001
$\widehat{\beta}_2$	0.0098	0.0140	0.4870
$\widehat{\beta}_3$	-0.0738	0.0140	< 0.001
Gamma regression model (robust estimators)			
$\widehat{\beta}_1$	5.5817	0.2558	< 0.001
$\widehat{\beta}_2$	-0.4396	0.3823	0.2500
$\widehat{\beta}_3$	2.6408	0.5209	< 0.001

2) OrbiSAR: The SAR image was acquired with the airborne OrbiSAR sensor of Bradar over São José dos Campos, Brazil. As reported in [43] and [44], the OrbiSAR is an airborne multipolarized dual-band SAR system of Bradar (formerly Orbisat), Brazil, which operates at the X-band with HH polarization and spatial resolution of 1 m and at the P-band with full polarization—HH, vertical (VV), VH, and HV—and spatial resolution of 2 m, with three antennas mounted on the same platform allowing repeat-pass and multibaseline interferometry, at P- and X-bands, respectively. The system is also equipped with a state-of-the-art navigation system and motion compensation [44]. In addition, the bandwidth and the radar swath can be up to 400 MHz and 14 km, respectively [44].

Fig. 4 shows an X-band SAR image acquired with the OrbiSAR system. The image is represented in a 2500×3150 matrix of magnitude data. The ground scene of the considered image is dominated by urban area (light ground–top and bottom right area), rivers (dark ground–bottom and left part of the image), forests, roads, and open areas (gray ground). The urban area presents a different pattern from the rest of the image and may be considered outliers.

To perform the ground type detection in the X-band SAR image, we adopted the same methodology described in the previous subsection to distinguish among an open area, a road, and an urban land type—referred to as Regions D, E, and F, respectively. Fig. 4 shows the three different evaluated regions.

Fig. 4. OrbiSAR image used in the regression models showing the tested regions. Regions D, E, and F represent an open area, a road, and an urban land type, respectively.

TABLE III
FIT REGRESSION MODELS FOR REGIONS D, E, AND F

	Estimate	Standard Error	p-value
Rayleigh regression model (robust estimators)			
$\widehat{\beta}_1$	-0.6069	0.0423	< 0.001
$\widehat{\beta}_2$	-0.1190	0.0598	0.0464
$\widehat{\beta}_3$	2.7767	0.1319	< 0.001
Rayleigh regression model (non-robust estimators)			
$\widehat{\beta}_1$	-0.6069	0.0423	< 0.001
$\widehat{\beta}_2$	-0.1105	0.0598	0.0646
$\widehat{\beta}_3$	2.6749	0.1319	< 0.001
Gaussian regression model (robust estimators)			
$\widehat{\beta}_1$	0.6087	0.1038	< 0.001
$\widehat{\beta}_2$	-0.0777	0.1468	0.5970
$\widehat{\beta}_3$	6.6209	0.3241	< 0.001
Gamma regression model (robust estimators)			
$\widehat{\beta}_1$	1.6312	0.0338	< 0.001
$\widehat{\beta}_2$	0.2542	0.0517	< 0.001
$\widehat{\beta}_3$	-1.5122	0.0346	< 0.001

The mean of the response signal was modeled using the model presented in (20), where the response signal is composed of the vectorized magnitude pixels of the Regions D, E, and F, and $x_2[n]$ and $x_3[n]$ are dummy variables related to regions E and F, respectively.

The fit models are shown in Table III, with $\delta = 0.001$ for the proposed method. The p-values show that all variables in Rayleigh and Gamma regression models considering a robust estimation process are significant for a probability of false alarm equal to 0.05, i.e., the null hypothesis in (21) can be rejected, indicating a correct detection of all evaluated ground types. In contrast, the variable $x_2[n]$ is not significant for the nonrobust Rayleigh regression method and robust Gaussian approach, i.e., these models cannot distinguish the road region, evidencing the importance of suitable models to deal with outliers in SAR image modeling.

B. Anomaly Detection

We propose a detection scheme to detect anomalies in an SAR image considering the Rayleigh regression model residuals. Our methodology aims at detecting area changes, measuring the deviations of the observed pixel values $y[n]$ from their estimated mean values $\widehat{\mu}[n]$. For such, we use the quantile residuals [28] that are defined as

$$r[n] = \Phi^{-1}\big(F(y[n]; \widehat{\mu}[n])\big) \tag{22}$$

where Φ^{-1} denotes the standard normal quantile function. The quantile residual can detect poor fitting in regression models and follows an approximately standard Gaussian distribution [28] if the model is correctly specified. If the estimated mean of the response signal is too far from the observed pixel value—which can be highlighted by the residual values—and then, an anomaly is detected. To capture a model mismatch, we adopt residual-based control charts that have been already used in change detection in remote sensing data, e.g., in [33] and [45]. The introduced anomaly detection methodology is based on the following premises.

1) If the model is correctly fit, then it is expected that the residuals are randomly distributed around zero and inside the interval $[-3, 3]$, about 99.7% of the observations $(2\Phi L) \ -1|_{L=3} \approx 99.7\%)$. Consequently, the control limit L can be set equal to three [45], [46].
2) If the residual value is outside the interval $[-3, 3]$, then the analyzed pixel is understood to differ from the expected behavior according to the Rayleigh regression model fit in the region of interest, and consequently, an anomaly is detected.

A postprocessing step using mathematical morphological operations, such as erosion, dilation, opening, and closing operations, can be considered aiming at: 1) removing small spurious pixel groups that are regarded as noise and 2) preventing the splitting of the interest objects into multiple substructures [47]. The anomaly detection method used in the current experiment is summarized in Algorithm 1.

To perform the proposed detection method in a CARABAS II SAR image, we selected a region containing military vehicles (anomalies), as shown in the dark gray rectangle in Fig. 3. This region has about 5% of the observations related to outliers. According to the Monte Carlo simulations, the WMLEs in the Rayleigh regression model are not strongly influenced by the presence or absence of outliers in the observed signal. In addition, because, in practical situations, it is difficult to identify whether there are outliers or not in the training sample, we selected as $\mathbf{X}_S$ a region with anomaly observations to highlight the importance of using a robust approach to deal with outliers.

To fit the regression model, we considered as covariates the other three images with the same flight pass available in the CARABAS II dataset to describe the amplitude mean value of the CARABAS II image pixels. The model is specified for

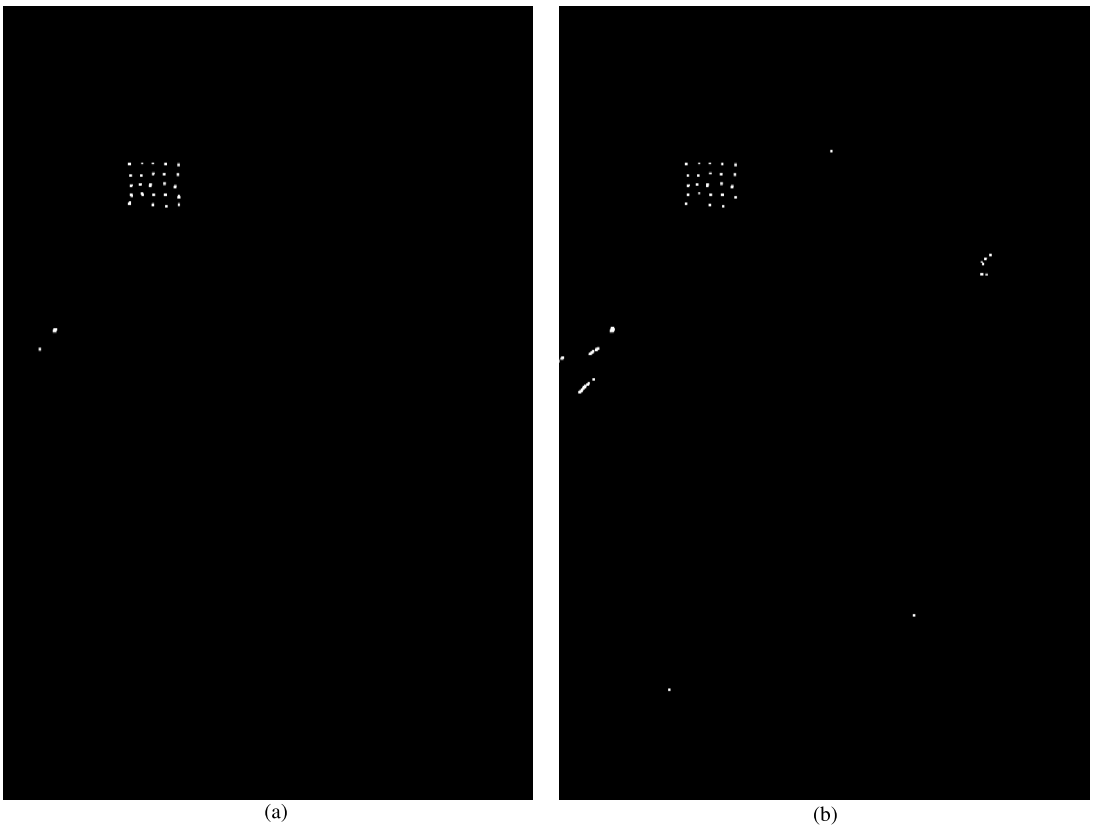

(a) (b)

Fig. 5. Detection results based on the robust and nonrobust estimation of the Rayleigh regression model parameters. (a) Detections: robust-based estimation. (b) Detections: nonrobust-based estimation.

Algorithm 1 Anomaly Detection Method Based on the Robust Rayleigh Regression Method

Require: Interest image $\mathbf{X}_{\mathrm{I}}$
Ensure: Detected results $\mathbf{X}_{\mathrm{D}}$
1) Select a region of interest (training sample) $\mathbf{X}_{\mathrm{S}} \subset \mathbf{X}_{\mathrm{I}}$.
2) Fit the robust Rayleigh regression method considering the $\mathbf{X}_{\mathrm{S}}$ image.
3) Using the fit model obtained in 2), compute the residuals $r[n]$ of $\mathbf{X}_{\mathrm{I}}$.
4) Obtain a binary images as follows:
if $(r[n] \leq L)$ or $(r[n] \geq L)$ **then**
$X^{\star}[n] \leftarrow 1$
else
$X^{\star}[n] \leftarrow 0$.
end if
5) Apply morphological operators as a final postprocessing step: $\mathbf{X}_{\mathrm{D}} \leftarrow \mathrm{postprocessing}(\mathbf{X}^{\star})$.

the response signal mean as follows:

$$g(\mu[n]) = \beta_1 + \beta_2 x_2[n] + \beta_3 x_3[n] + \beta_4 x_4[n]. \qquad (23)$$

The response signal is composed of the vectorized amplitude values of the training sample pixels. Variables $x_2[n]$, $x_3[n]$, and $x_4[n]$ are the vectorized magnitude pixels of the images related to pass one and missions two, three, and four, respectively. As we expect to have outliers in the observed signal and not in the covariates, $x_2[n]$, $x_3[n]$, and $x_4[n]$ represent a forest area. For the postprocessing step, we employed an opening operation—considering a 3×3 pixels square structuring element, whose size is linked by the system resolution followed by a dilation—using 7×7 pixels structuring element, which is related to the approximate size of the military vehicles. Using such operations, we kept the criterion defined in [6], i.e., detections with less than 10 m apart are merged as one.

The anomaly detection results can be found in Fig. 5. We compared the detection results of the Rayleigh regression models considering a robust and nonrobust estimation process, which are displayed in Fig. 5. The robust method detected 24 military vehicles and two false alarms. In contrast, the nonrobust scheme can only detect 23 military vehicles and shows 15 false alarms. In particular, the false alarms in the nonrobust method are related to the power lines area; this result is in accordance with the ones presented in the Section IV-A, showing that, in both experiments, the nonrobust estimation process cannot distinguish between the targets and power line areas, and consequently, evidencing the importance of a robust approach to deal with outliers.

We also compared the proposed methodology with three different approaches presented in [5], [6], and [26]; the performance of the proposed scheme was very close to the competing methods specifically developed to this aim: only one less detection hit; and two more false alarms than the results showed in [5] and [26]. On the one hand, the accurate

TABLE IV
NUMBER OF DETECTED TARGETS AND FALSE ALARMS OBTAINED CONSIDERING THE RAYLEIGH REGRESSION MODELS BASED ON ROBUST AND NONROBUST APPROACHES, AND THE METHODS IN [5], [6], AND [26]

Method	Detected Targets	False Alarm
Robust Approach	24	2
Non-robust Approach	24	15
Method in [5]	25	0
Method in [6]	25	2
Method in [26]	25	0

performance of such methods is related to an optimized threshold choice. On the other hand, our proposed anomaly detection method shows accurate detection results avoiding this step since the residual-based control chart has a fixed theoretical threshold ($L = 3$). The detection results of all evaluated methods are summarized in Table IV.

V. CONCLUSION

This article introduced robust estimators for the Rayleigh regression model parameters. In particular, we employed the weighted maximum likelihood approach to obtain estimators that are robust to the presence of outliers. Monte Carlo simulation results showed that the WMLEs outperformed traditional MLEs in terms of relative bias and root mean square error. In particular, the nonrobust estimators presented a relative bias value 65-fold larger than the results provided by the robust estimators in signals corrupted with outliers. In terms of sensitivity analysis and break down point, the robust approach resulted in a reduction of about 96% and 10% in the mean absolute value in compassion to the nonrobust estimators. For noncontaminated signals, both schemes had similar behavior. Two studies considering the proposed robust approach in the Rayleigh regression model parameter estimation to distinguish between different regions in an SAR image were presented and discussed, showing competitive detection results compared to the nonrobust Rayleigh-, robust Gaussian-, and robust Gamma-based measurements. Moreover, we proposed an anomaly detector based on the Rayleigh regression model. The robust estimation approach exceled in terms of detection compared to the nonrobust estimators of the Rayleigh regression model parameters, and it offered very close results to those reported in [5], [6], and [26], i.e., only one less detection hit, and two more false alarms than the results showed in [5] and [26].

REFERENCES

[1] C. Oliver and S. Quegan, *Understanding Synthetic Aperture Radar Images*. Rijeka, Croatia: SciTech, 2004.

[2] G. Melamed, S. R. Rotman, D. G. Blumberg, and A. J. Weiss, "Anomaly detection in polarimetric radar images," *Int. J. Remote Sens.*, vol. 33, no. 4, pp. 1164–1189, Feb. 2012.

[3] F. E. Grubbs, "Procedures for detecting outlying observations in samples," *Technometrics*, vol. 11, no. 1, pp. 1–21, 1969.

[4] O. H. Bustos, M. Lucini, and A. C. Frery, "M-estimators of roughness and scale for-modelled SAR imagery," *EURASIP J. Adv. Signal Process.*, vol. 2002, no. 1, Dec. 2002, Art. no. 297349.

[5] B. G. Palm *et al.*, "Wavelength-resolution SAR ground scene prediction based on image stack," *Sensors*, vol. 20, no. 7, p. 2008, Apr. 2020.

[6] M. Lundberg, L. M. H. Ulander, W. E. Pierson, and A. Gustavsson, "A challenge problem for detection of targets in foliage," *Proc. SPIE, Algorithms Synth. Aperture Radar Imag. XIII*, vol. 6237, May 2006, Art. no. 62370K.

[7] O. Bustos, S. Ojeda, and R. Vallejos, "Spatial ARMA models and its applications to image filtering," *Brazilian J. Probab. Statist.*, vol. 23, no. 2, pp. 141–165, Dec. 2009.

[8] H. Sportouche, J.-M. Nicolas, and F. Tupin, "Mimic capacity of Fisher and generalized gamma distributions for high-resolution SAR image statistical modeling," *IEEE J. Sel. Topics Appl. Earth Observ. Remote Sens.*, vol. 10, no. 12, pp. 5695–5711, Dec. 2017.

[9] C. Tison, J. M. Nicolas, F. Tupin, and H. Maître, "A new statistical model for Markovian classification of urban areas in high-resolution SAR images," *IEEE Trans. Geosci. Remote Sens.*, vol. 42, no. 10, pp. 2046–2057, Oct. 2004.

[10] J. Inglada and G. Mercier, "A new statistical similarity measure for change detection in multitemporal SAR images and its extension to multiscale change analysis," *IEEE Trans. Geosci. Remote Sens.*, vol. 45, no. 5, pp. 1432–1445, May 2007.

[11] G. Mercier, G. Moser, and S. B. Serpico, "Conditional copulas for change detection in heterogeneous remote sensing images," *IEEE Trans. Geosci. Remote Sens.*, vol. 46, no. 5, pp. 1428–1441, May 2008.

[12] Y. Zhao, B. Huang, and H. Song, "A robust adaptive spatial and temporal image fusion model for complex land surface changes," *Remote Sens. Environ.*, vol. 208, pp. 42–62, Apr. 2018.

[13] H. Allende, J. Galbiati, and R. Vallejos, "Robust image modeling on image processing," *Pattern Recognit. Lett.*, vol. 22, no. 11, pp. 1219–1231, Sep. 2001.

[14] J. Naranjo-Torres, J. Gambini, and A. C. Frery, "The geodesic distance between $\mathcal{G}_i^0$ models and its application to region discrimination," *IEEE J. Sel. Topics Appl. Earth Observ. Remote Sens.*, vol. 10, no. 3, pp. 987–997, Mar. 2017.

[15] H. Wang and K. Ouchi, "Accuracy of the K-distribution regression model for forest biomass estimation by high-resolution polarimetric SAR: Comparison of model estimation and field data," *IEEE Trans. Geosci. Remote Sens.*, vol. 46, no. 4, pp. 1058–1064, Apr. 2008.

[16] A. M. Zoubir, V. Koivunen, E. Ollila, and M. Muma, *Robust Statistics for Signal Processing*. Cambridge, U.K.: Cambridge Univ. Press, 2018.

[17] B. G. Palm, F. M. Bayer, R. J. Cintra, M. I. Pettersson, and R. Machado, "Rayleigh regression model for ground type detection in SAR imagery," *IEEE Geosci. Remote Sens. Lett.*, vol. 16, no. 10, pp. 1660–1664, Oct. 2019.

[18] P. McCullagh and J. Nelder, *Generalized Linear Models*, 2nd ed. London, U.K.: Chapman & Hall, 1989.

[19] A. Ghosh and A. Basu, "Robust estimation in generalized linear models: The density power divergence approach," *Test*, vol. 25, no. 2, pp. 269–290, Jun. 2016.

[20] A. Ghosh and A. Basu, "Robust estimation for independent non-homogeneous observations using density power divergence with applications to linear regression," *Electron. J. Statist.*, vol. 7, pp. 2420–2456, Jan. 2013.

[21] J. Susaki, K. Hara, K. Kajiwara, and Y. Honda, "Robust estimation of BRDF model parameters," *Remote Sens. Environ.*, vol. 89, no. 1, pp. 63–71, Jan. 2004.

[22] A. M. Zoubir, "Introduction to statistical signal processing," in *Academic Press Library in Signal Processing*, vol. 3. Amsterdam, The Netherlands: Elsevier, 2014, pp. 3–7.

[23] C. Field and B. Smith, "Robust estimation: A weighted maximum likelihood approach," *Int. Stat. Rev.*, vol. 62, no. 3, pp. 405–424, 1994.

[24] L. M. H. Ulander, M. Lundberg, W. Pierson, and A. Gustavsson, "Change detection for low-frequency SAR ground surveillance," *IEE Proc.-Radar, Sonar Navigat.*, vol. 152, no. 6, pp. 413–420, Dec. 2005.

[25] V. T. Vu, "Wavelength-resolution SAR incoherent change detection based on image stack," *IEEE Geosci. Remote Sens. Lett.*, vol. 14, no. 7, pp. 1012–1016, Jul. 2017.

[26] V. T. Vu, N. R. Gomes, M. I. Pettersson, P. Dammert, and H. Hellsten, "Bivariate gamma distribution for wavelength-resolution SAR change detection," *IEEE Trans. Geosci. Remote Sens.*, vol. 57, no. 1, pp. 1–9, Aug. 2018.

[27] L. Devroye, "Sample-based non-uniform random variate generation," in *Proc. 18th Conf. Winter Simulation (WSC)*, 1986, pp. 260–265.

[28] P. K. Dunn and G. K. Smyth, "Randomized quantile residuals," *J. Comput. Graph. Statist.*, vol. 5, no. 3, pp. 236–244, Sep. 1996.

[29] W. Press, S. Teukolsky, W. Vetterling, and B. Flannery, *Numerical Recipes in C: The Art of Scientific Computing*. Cambridge, U.K.: Cambridge Univ. Press, 2 ed., 1992.

[30] F. Hu and J. V. Zidek, "The weighted likelihood," *Can. J. Statist.*, vol. 30, no. 3, pp. 347–371, 2002.
[31] S. M. Kay, *Fundamentals of Statistical Signal Processing: Detection Theory*, vol. 2. Upper Saddle River, NJ, USA: Prentice-Hall, 1998.
[32] H. Allende and L. Pizarro, "Robust estimation of roughness parameter in SAR amplitude images," in *Proc. Iberoamerican Congr. Pattern Recognit.* Berlin, Germany: Springer, 2003, pp. 129–136.
[33] D. M. Bayer, F. M. Bayer, and P. Gamba, "A 3-D spatiotemporal model for remote sensing data cubes," *IEEE Trans. Geosci. Remote Sens.*, vol. 59, no. 2, pp. 1082–1093, Feb. 2021.
[34] F. R. Hampel, "A general qualitative definition of robustness," *Ann. Math. Statist.*, vol. 42, no. 6, pp. 1887–1896, 1971.
[35] V. J. Yohai, "High breakdown-point and high efficiency robust estimates for regression," *Ann. Statist.*, vol. 15, no. 2, pp. 642–656, 1987.
[36] SDMS. (2018). *Sensor Data Management System Public Web Site*. [Online]. Available: https://www.sdms.afrl.af.mil/index.php
[37] P. Rousseeuw *et al.* (2020). *Robustbase: Basic Robust Statistics*. R Package Version 0.4-5. [Online]. Available: http://CRAN.R-project.org/package=robustbase
[38] R. A. Fisher, "Statistical methods for research workers," in *Breakthroughs in Statistics*. New York, NY, USA: Springer, 1992, pp. 66–70.
[39] L. Sevgi, "Hypothesis testing and decision making: Constant-false-alarm-rate detection," *IEEE Antennas Propag. Mag.*, vol. 51, no. 3, pp. 218–224, Jun. 2009.
[40] X. Ru, Z. Liu, Z. Huang, and W. Jiang, "Normalized residual-based constant false-alarm rate outlier detection," *Pattern Recognit. Lett.*, vol. 69, pp. 1–7, Jan. 2016.
[41] S. Maleki, S. P. Chepuri, and G. Leus, "Energy and throughput efficient strategies for cooperative spectrum sensing in cognitive radios," in *Proc. IEEE 12th Int. Workshop Signal Process. Adv. Wireless Commun.*, Jun. 2011, pp. 71–75.
[42] P. Weber, D. Theilliol, C. Aubrun, and A. Evsukoff, "Increasing effectiveness of model-based fault diagnosis: A dynamic Bayesian network design for decision making," *IFAC Proc. Volumes*, vol. 39, no. 13, pp. 90–95, Aug. 2007.
[43] T. L. M. Barreto *et al.*, "Classification of detected changes from multitemporal high-res Xband SAR images: Intensity and texture descriptors from superpixels," *IEEE J. Sel. Topics Appl. Earth Observ. Remote Sens.*, vol. 9, no. 12, pp. 5436–5448, Dec. 2016.
[44] G. H. X. Shiroma, K. A. C. de Macedo, C. Wimmer, J. R. Moreira, and D. Fernandes, "The dual-band polInSAR method for forest parametrization," *IEEE J. Sel. Topics Appl. Earth Observ. Remote Sens.*, vol. 9, no. 7, pp. 3189–3201, Jul. 2016.
[45] E. B. Brooks, R. H. Wynne, V. A. Thomas, C. E. Blinn, and J. W. Coulston, "On-the-fly massively multitemporal change detection using statistical quality control charts and landsat data," *IEEE Trans. Geosci. Remote Sens.*, vol. 52, no. 6, pp. 3316–3332, Jun. 2014.
[46] F. M. Bayer, A. J. Kozakevicius, and R. J. Cintra, "An iterative wavelet threshold for signal denoising," *Signal Process.*, vol. 162, pp. 10–20, Sep. 2019.
[47] R. C. Gonzalez and R. Woods, *Digital Image Processing*. Upper Saddle River, NJ, USA: Prentice-Hall, 2008.

Bruna G. Palm received the B.Sc. degree in statistics from Federal University of Santa Maria (UFSM), Santa Maria, Brazil, in 2014, and the D.Sc. degree in statistics from Federal University of Pernambuco (UFPE), Recife, Brazil, in 2020.

From February 2018 and January 2019, she was a Guest Ph.D. Researcher with Blekinge Institute of Technology (BTH), Karlskrona, Sweden. She was a Research Fellow with the Department of Telecommunications, Aeronautics Institute of Technology (ITA), São José dos Campos, Brazil, from April 2020 to March 2021. She is currently a Research Fellow with BTH in partnership with Saab AB, Sweden. Her research interests include data science, regression/dynamic models, statistical computing, parametric inference, and statistical signal/image processing.

Fábio M. Bayer (Member, IEEE) received the B.Sc. degree in mathematics from Federal University of Santa Maria (UFSM), Santa Maria, Brazil, in 2006, and the D.Sc. degree in statistics from Federal University of Pernambuco (UFPE), Recife, Brazil, in 2011.

In 2019, he was a Visiting Researcher with the Telecommunications and Remote Sensing Laboratory, University of Pavia, Pavia, Italy. He is currently an Associate Professor with the Department of Statistics, UFSM, and a Researcher with the Santa Maria Space Science Laboratory (LACESM), UFSM. His research interests include data science, regression and dynamic models, statistical computing, parametric inference, and statistical signal processing.

Mr. Bayer also serves as a Topical Associate Editor for the IEEE TRANSACTIONS ON GEOSCIENCE AND REMOTE SENSING in the general area of statistical signal processing.

Renato Machado (Senior Member, IEEE) received the B.S.E.E. degree from São Paulo State University (UNESP), Ilha Solteira, Brazil, in 2001, and the M.Sc. and Ph.D. degrees in electrical engineering from Federal University of Santa Catarina (UFSC), Florianópolis, Brazil, in 2004 and 2008, respectively.

He was a visiting Ph.D. Scholar with the Department of Electrical Engineering, Arizona State University, Tempe, AZ, USA, from August 2006 to June 2007. From November 2013 to February 2015, he was a visiting Research Fellow with Blekinge Institute of Technology (BTH), Karlskrona, Sweden, in partnership with Saab AB, Sweden. He worked with the Research and Development Department, Nokia Institute of Technology, Brasılia, Brazil, from 2007 to 2008. From August 2009 to December 2017, he was an Assistant Professor from 2008 to 2016 and an Associate Professor in 2017 with the Federal University of Santa Maria, Santa Maria, Brazil, where he lectured many courses to bachelor's and graduate programs and assumed different positions in the institution, namely, a Researcher Leader of the Communications and Signal Processing Research Group, a Coordinator of the Telecommunications Engineering Program, and the Director of the Aerospace Science Laboratory. Since December 2017, he has been an Associate Professor with the Aeronautics Institute of Technology (ITA), São José dos Campos, Brazil. He is currently the Research Leader of the Digital and Signal Processing Laboratory, ITA, and the SAR and Radar Signal Processing Laboratory, ITA. His research interests include SAR processing, SAR image processing, change detection, radar signal processing, and digital signal processing.

Mats I. Pettersson (Senior Member, IEEE) received the M.Sc. degree in engineering physics, the Licentiate degree in radio and space science, and the Ph.D. degree in signal processing from Chalmers University of Technology, Gothenburg, Sweden, in 1993, 1995, and 2000, respectively.

For some years, he worked with mobile communication research at Ericsson, Sweden. For ten years, he was employed with the Swedish Defence Research Agency (FOI), Sweden. At FOI, he was focusing on ultrawideband low-frequency SAR systems. Since 2005, he has been employed with Blekinge Institute of Technology (BTH), Karlskrona, Sweden, where he is currently a Full Professor and the Research Director. His work is related to remote sensing, where his research interests include SAR inversion and processing, space–time adaptive processing (STAP), high-resolution SAR change detection, automotive radar, and radio occultation.

Dr. Pettersson is also a member of the BTH Board of Governors.

Viet T. Vu (Senior Member, IEEE) was born in Hanoi, Vietnam. He received the Diploma degree in electronics from Hanoi University of Technology, Hanoi, Vietnam, in 1999, the M.Sc. degree in communication engineering from the University of Duisburg-Essen, Duisburg, Germany, in 2004, and the Licentiate degree in applied signal processing and the Ph.D. degree in applied signal processing from Blekinge Institute of Technology (BTH), Karlskrona, Sweden, in 2009 and 2011, respectively.

He became an Assistant Professor at BTH in 2016. His research interests include mono- and bi-static SAR signal processing, applications of SAR in change detection, moving target detection and estimation, and radio occultation.

Renato J. Cintra (Senior Member, IEEE) received the Ph.D. degree in electrical engineering from the Universidade Federal de Pernambuco (UFPE), Recife, Brazil, in 2005.

He joined as a Faculty Member at the Centre for Natural and Exact Sciences, UFPE, in 2005. He held visiting scholar appointments at The University of Akron, Akron, OH, USA; the Département Informatique, INSA Lyon, Villeurbanne, France; the INRIA/IRISA Lab, University of Rennes 1, Rennes, France; the University of Calgary, Calgary, AB, Canada; and Florida International University, Miami, FL, USA. His research interests include approximation theory for discrete transforms, theory and methods for digital signal/image processing, computationally efficient statistical algorithms, and probabilistic methods.

Dr. Cintra was an Associate Editor for IEEE GEOSCIENCE REMOTE SENSING LETTERS, *IET Circuits, Devices & Systems*, and *Circuits, Systems, and Signal Processing* (Springer). He currently serves as an Associate Editor for the *Journal of Communication and Information Systems* and a Subject Editor for *Electronics Letters*.